energies

MDPI

*Article*

# *Cost-efficient*, Effect of Low-Quality $PbI_2$ Purification to Enhance Performances of Perovskite Quantum Dots and Perovskite Solar Cells

**ChaeHyun Lee [1], YeJi Shin [1], Gyeong G. Jeon [2], Dongwoo Kang [3], Jiwon Jung [3], Byeongmin Jeon [3], Jongin Park [3,*], Jincheol Kim [2,*] and Seog Joon Yoon [1,*]**

1 Department of Chemistry, College of Natural Science, Yeungnam University, 280 Daehak-Ro, Gyeongsan, Gyeongbuk 38541, Korea; dwuos@naver.com (C.L.); aashinyj@naver.com (Y.S.)
2 New & Renewable Energy Research Center, Korea Electronics Technology Institute, Seong-Nam 13509, Korea; eastjk2@keti.re.kr
3 Daegu Science High School, 154, Dongdaegu-ro, Daegu 42110, Korea; ts19048@ts.hs.kr (D.K.); ts19078@ts.hs.kr (J.J.); ts19077@ts.hs.kr (B.J.)
* Correspondence: kisses84@ts.hs.kr (J.P.); jckim@keti.re.kr (J.K.); yoon@yu.ac.kr (S.J.Y.)

**Abstract:** In modern society, high-quality material development and a large stable supply are key to perform frontier research and development. However, there are negative issues to address to utilize high-quality resources with a large stable supply for research, such as economic accessibility, commercialization, and so on. One of the cutting-edge research fields, perovskite-related research, usually requires high-quality chemicals with outstanding purity (>99%). We developed an economically feasible $PbI_2$ precursor with around 1/20 cost-down for perovskite/perovskite quantum dots through recrystallization and/or hydrothermal purification. Following the methodology, the quantum dots from both as-prepared and purified $PbI_2$ demonstrated identical photophysical properties, with a photoluminescence quantum yield (PLQY) of 52.61% using the purified $PbI_2$ vs. 45.83% PLQY using commercial $PbI_2$. The role of hydrothermal energy was also checked against the problematic $PbI_2$, and we checked whether the hydrothermal energy could contribute to the hindrance of undesired particle formation in the precursor solution, which enables them to form enlarged grain size from 179 $\pm$ 80 to 255 $\pm$ 130 nm for higher photoconversion efficiency of perovskite solar cells from 14.77 $\pm$ 1.82% to 15.18 $\pm$ 1.92%.

**Keywords:** perovskite; perovskite quantum dots; perovskite solar cells; hydrothermal; perovskite precursor purification



**Citation:** Lee, C.; Shin, Y.; Jeon, G.G.; Kang, D.; Jung, J.; Jeon, B.; Park, J.; Kim, J.; Yoon, S.J. *Cost-efficient*, Effect of Low-Quality $PbI_2$ Purification to Enhance Performances of Perovskite Quantum Dots and Perovskite Solar Cells. *Energies* **2021**, *14*, 201. https://doi.org/10.3390/en14010201

Received: 26 November 2020
Accepted: 25 December 2020
Published: 2 January 2021



## 1. Introduction

In modern research and development (R&D), high-quality products usually require high-quality resources with very low impurity. Current chemical industries successfully developed various strategies to provide high-quality chemicals with high purities up to 99.999% in general, or even higher purities. For example, some modern researchers can purchase high-quality chemicals for their research to elucidate the effect of impurities [1], doping [2], regional deformation [3], or to aim at high performances of various electronic/optoelectronic devices [4]. Limiting impurities in the stage of material synthesis or device fabrication is essential to control experimental factors. This variable control should be performed to reduce negative aspects in numerous R&D fields: byproducts in synthesis, current loss, and/or short circuit current in electronic devices, and non-radiative recombination sites in optoelectronic devices. The market for supplying high-quality chemicals is inevitable for cutting-edge R&D and industrial processes.

Some of the negative aspects of the supply of high-quality chemicals are economic accessibility, production costs, commercialization, and the supply of large amounts for industrial processes. Usually, scientists and engineers need to spend more to obtain

the same amount of chemicals with higher purities. This trend gets worse when the researchers would like to purchase ultra-high-quality chemicals with >99.99% purities or higher. Economically, researchers who had limited research funding do not have an equal chance to obtain high-quality resources, which are essential for the frontier R&D, compared to those who can perform research with sufficient funding. The expensive chemicals required for higher purity can induce economic inaccessibility, so the uneven opportunity to perform cutting-edge R&D can be derived. In addition, usage of the high-cost resources increases production costs, so the price of alternative devices can limit their commercialization. Beyond the large-scale production, the consumption of a larger amount of chemicals is essential, but the sustainable supply of the high purity chemicals is often one of the general issues for large-scale production [5]. For the frontier R&D and industrial process, it is still essential to develop purification strategies to use economic chemicals with low quality and prove the similarity by using two low-and-high purity chemicals so that we can achieve equal opportunity for all researchers with different funding situations, reducing production costs for commercialization, and a sustainable supply for the industrial process.

One of the cutting-edge R&D fields is research about the organic–inorganic hybrid $ABX_3$ (A = $MA^+$, $FA^+$, and $Cs^+$, where $MA^+$: methylammonium, $FA^+$: formamidinium, B = $Pb^{2+}$ and $Sn^{2+}$, and X = $Cl^-$, $Br^-$, and $I^-$) perovskites. Ever since the pioneering research of Mitzi and coworkers was published [6–8], research about hybrid perovskites has been published since the early 21st century with a drastic photoconversion efficiency increment of perovskite solar cells (PSCs) in 11 years, from 3.8% [9] to 25.17% [4], which overcomes the minimum efficiency (~19%) for commercialization. This is because there are positive potentials of the perovskite, such as fast charge transport [10], long diffusion length (up to few micrometers [11]), high absorption cross-sections comparable to various outstanding photosensitizers [12], and low exciton binding energies (16–32 meV) [13], which are similar to thermal energy ($k_bT$) at room temperature for the efficient charge separation in the PSCs. Researchers have used precursors with the best qualities to maximize the perovskite potentials, for example, >99.99% for $PbI_2$ precursor [4]. Furthermore, various techniques to improve the quality of material have been applied to achieve higher photophysical properties and/or photoconversion efficiency of PSCs, such as anti-solvent engineering [14], perovskite powder preparation and crystallization [15], inverse recrystallization [16], single crystal growth [17], incorporation of mixing A-site cations [18] and/or X-site anions [19], and so on. In short, the cutting-edge research field for perovskites has also been focused on the development of high-quality perovskite materials using ultra-high purity of precursors. This is because small impurities, hydrated sources, and stabilizers can induce various trap states, which can act as non-radiative recombination sites; these sites can decrease the charge carrier's lifetime, photoluminescence quantum yield (PLQY), and photoconversion efficiency in PSCs [1,15,20].

The drastic improvement of PSCs' performance attracts researchers to utilize the perovskite in various fields, such as light-emitting diodes (LEDs) [21], lasers [22], photocatalysis [23], hydrogen-evolution reactors [24], non-linear optics [25], and so on. For the application of the perovskites to the various fields, various factors were controlled, such as dimensionalities (3D bulk film [14], 2D nanosheet [26], 1D nanowire [27], and 0D quantum dots [25,28]), compositions [18,19], crystallinities [17], and so on. Among the various dimensional perovskites, 0D perovskite quantum dots (PQDs) were widely used with outstanding PLQY (>90%) [29] due to the preferred major radiative recombination process (as opposed to the less preferred minor non-radiative recombination process).

Considering the aspects mentioned earlier, such as economic accessibility, commercialization, large-scale production, and importance of the key material quality improvement, it is necessary to develop strategies to improve the quality of perovskite precursor from low-grade economic sources for better perovskite/perovskite quantum dot quality. In this work, we used economically low-grade chemicals to synthesize one of the key precursors for perovskite/PQDs, $PbI_2$. Through additional recrystallization and consecutive hydrothermal process, with the purified $PbI_2$, we could obtain similar PLQY compared to high-cost

$PbI_2$ with 99.99% purity (purchased from TCI®). The hydrothermal also applied to another high purity $PbI_2$ with 99.9985% (purchased from Alfa Aesar®) purity and with undesired dissolution issue at certain reaction batch (LOT:U14E066). Through hydrothermal using the issued $PbI_2$, we solved the dissolution issue with enlarged grain and slight improvement of photoconversion efficiency. Our work could provide a practical solution for the researchers to obtain better $PbI_2$ precursors from economically approachable low-grade sources, which acts like high-quality $PbI_2$.

## 2. Materials and Methods

### *2.1. Materials*

#### 2.1.1. Materials for Perovskite Precursors and Perovskite Quantum Dots

Lead acetate ($Pb(CH_3CO_2)_2$, Fisher Chemical, 6080-56-4, 99.5%), Potassium iodide (KI, Samchun Chemicals, 7681-11-0, 99.5%) and Hydrochloric acid (HCl, Daejung Chemicals, 7647-01-0, 35.0%) for Lead iodide synthesis

All reagents except $PbI_2$ were used as received without further purification: $PbI_2$ (lead(II) iodide 99.999%, 10101-63-0, TCI), Cesium carbonate ($Cs_2CO_3$, Daejung, 534-17-8, 99.5%), Oleic acid (OA, Alfa aesar, 112-80-1, 90%), 1-octadecene (Sigma-Aldrich, 112-88-9, 90%), Oleylamine (OLA, TCI, 112-90-3, 50%), n-hexane (Daejung, 110-54-3, 95%), Molecular sieves 4 A, 4–8 mesh (Samchun, 70955-01-0) and riboflavin (Daejung, 83-88-5, 98%) were used to synthesized perovskite quantum dots and analyzed properties. 1-Octadecene was heated at 120 °C for 2 h to remove the dissolved oxygen. In the case of hexane, Molecular sieves 4 Å, 4-8 mesh were used to eliminate water, and other solutions also used nitrogen purge to stabilize the synthesis of quantum dots.

#### 2.1.2. Materials for Perovskite Solar Cells

The $SnO_2$ colloid precursor (tin (IV) oxide, 15% in $H_2O$ colloidal dispersion, product # 44592) and $PbI_2$ (99.9985%, product # 12724, Lot # U14E066) were purchased from Alfa Aesar. Bis(trifluoromethylsulfonyl)imide lithium salt (Li-TFSI, product # 449504), acetonitrile (99.8%, anhydrous, product # 271004), 4-tert-butylpyridine (t-BP, 98%, product # 142379), N,N-dimethylformamide (DMF, 99.8%, anhydrous, product # 227056), dimethyl sulfoxide (DMSO, 99.9%, anhydrous, product # 276855), and chlorobenzene (CB, 99.8%, anhydrous, product # 284513) were purchased from Sigma-Aldrich. Methylammonium iodide (MAI, 99.99%, product # MS101000) was purchased from Greatcell Solar. The 2,2′,7,7′-tetrakis(N,N-dip-methoxyphenylamine)-9,9′-spirobifluorene (Spiro-OMeTAD, 99.5%, product # LT-S922) was purchased from Lumtech.

### *2.2. Methods*

#### 2.2.1. Methods for Lead Iodide Synthesis and Purification

First, 3.793 g lead acetate and 5.29 g potassium iodide were dissolved in 1 L distilled water each. Continuously addition of 3 mL of 4 M Hydrochloric acid to lead acetate solution could prevent its hydrolysis. We mixed the two aqueous solutions gradually with few drops early. As soon as bright yellow lead iodide precipitate was observed in the mixing process. After the precipitate is formed, we heated the remaining solution until the $PbI_2$ precipitate was dissolved to induce recrystallization. After the observing clean solution, the heat was turned off and then the heated solution was cooled down to room temperature on its own (~2h). Around 2 h later, recrystallized $PbI_2$ was formed. When the $PbI_2$ solution's temperature was stabilized, it was placed into a fridge for 3 h to obtain as much $PbI_2$ from the solution as possible. Recrystallized $PbI_2$ was consecutively filtered to isolate the $PbI_2$. The $PbI_2$ was dried overnight in a vacuum. Furthermore, hydrothermal was performed after the drying process, according to methods found in the literature [30]. In short, 0.8 g of Lead iodide and 120 mL of DI-water were placed in a 150 mL Teflon-lined Hydrothermal autoclave. We maintained the autoclave at 200 °C for 6 h and then cooled the solution at room temperature; the crystallized $PbI_2$ was filtered out and dried in a vacuum oven overnight [30].

#### 2.2.2. Synthesis of $CsPbI_3$ Perovskite Quantum Dots

**Cs oleate synthesis**: 0.407 g of $Cs_2CO_3$, 1.25 mL of oleic acid (OA) and 20 mL of octadecene (ODE) were placed in a 50 mL three-neck flask and heated to 80 °C for 1 h in a vacuum to remove any water. Then, the temperature was kept at 120 °C for 1 h. The Cs precursor was raised to 140 °C under $N_2$ until all $Cs_2CO_3$ reacted with OA and then naturally cooled to 115 °C.

**Pb precursor synthesis**: a mixture of ODE (25 mL) and 0.5 g $PbI_2$ was put in another three-neck flask, and the system was degassed under vacuum at 120 °C for 1 h. In addition, OA 2.5 mL and oleylamine (OLA) 2.5 mL were put in another beaker at 130 °C. After completely removing the water from $PbI_2$ and ODE, we injected the OA and OLA mixture into another three-neck flask. Afterwards, an injection vacuum was applied to remove the water.

**Hot injection**: The temperature in the three-neck flask containing ODE, $PbI_2$, OA, and OLA was adjusted in a nitrogen environment to 170 °C. When the temperature reached 170 °C, we injected 2 mL of Cs-oleate; we cooled down the temperature by putting an ice bath under the reacting flask. When the temperature reached 60 °C, the supernatant was obtained, and centrifugation at 6000 rpm for 10 min was used to obtain a precipitate of PQDs. The precipitate was obtained, and the PQDs precipitate was dissolved in 10 mL of hexane and $N_2$ purging for 5 min.

#### 2.2.3. Characterizations of $PbI_2$ Precursor and $CsPbI_3$ Perovskite Quantum Dots

TEM images and selective area electron diffraction patterns (SAED) were acquired using a Tecnai G2 F20 S-TWIN (FEI Korea). The XRD was performed using a D8 Advance (Bruker). The X-ray diffractometer was equipped with Cu K$\alpha$ radiation, 10-80° with 0.05 deg/step, 0.5 sec/step. UV-Vis absorption and photoluminescence spectrophotometer data were performed using Duetta (HORIBA Scientific). We used excitation light at 435 nm to excite PQDs to prevent overtone up to 800 nm and obtain pristine photoluminescence spectra of the PQDs. The PQDs were compared to the PLQY of riboflavin, as 0.3 [31] for measured PLQY. We used an excitation wavelength of 435 nm to obtain PLQY. X-ray fluorescence spectroscopic analysis (XRF) was characterized through NEX-CG (Rigaku) by fundamental parameter (FP) analysis with Energy-dispersive X-ray fluorescence (ED-XRF) semi-quantitative analytic method.

#### 2.2.4. Perovskite Solar Cell Fabrication and Photoconversion Efficiency Measurement

The patterned Fluorine-doped Tin Oxide (FTO) glass was cleaned by using ultrasonication for 15 min in detergent, deionized (DI) water, acetone, and isopropyl alcohol (IPA). Before use, the cleaned FTO glass was treated with UV/ozone for 20 min. The substrate was then spin-coated with $SnO_2$ solution (2.75% in DI water) at 3000 rpm for 30 s, annealed at 150 °C for 30 min, and UV/ozone treated for 20 min.

A perovskite precursor solution of $MAPbI_3$ (1.13 M) was prepared by dissolving $PbI_2$ and MAI in a mixed solvent of *N*,*N*-dimethylformamide (DMF): dimethyl sulfoxide (DMSO) = 4:1 (volume ratio) and heated at 60 °C for 20 min before using. The precursor solution was spin-coated onto $SnO_2$ at 1000 rpm for 5 s and 5000 rpm for 50 s. In the second step, 600 µL of CB was smoothly dropped on the film when 45 s of the spinning remained. After deposition, the film was annealed at 100 °C for 15 min in an $N_2$-filled glove box. The spiro-OMeTAD solution was then prepared by dissolving 91 mg spiro-OMeTAD in 1 mL chlorobenzene after adding 20.9 µL of Li-TFSI in acetonitrile (517 mg/mL) and 35.4 µL of t-BP and spin-coated at 4000 rpm for 30 s. As a counter electrode, 100 nm of Au was deposited by thermal evaporated through a shadow mask under a high vacuum condition (under $10^{-5}$ torr).

Current density-voltage curves (J-V curves) were measured using Keithley 2602A Source Meter under simulated air mass (AM) 1.5 G illumination (100 mW $cm^{-2}$) with a solar simulator (K3000 model, McScience) calibrated using a standard Si reference cell

(K801S-K067, McScience). The effective area of devices was 0.875 $cm^2$ using a patterned mask during measurement.

## 3. Results and Discussion

### *3.1. $PbI_2$ Synthesis and Purification Using Economical Low-Grade Sources*

To obtain economically feasible $PbI_2$ with affordable quality, by obtaining motivation from *"Golden Rain"*, provided *Royal Society of Chemistry*, we modified the experiment to synthesize $PbI_2$ using a precipitation reaction (details in Section 2) [32], as follows:

$$Pb(CH_3COO)_{2\ (aq)} + 2KI_{(aq)} \rightarrow PbI_{2\ (s)} + 2(CH_3COO)_{2\ (aq)} \quad (1)$$

Furthermore, we performed recrystallization and consecutive hydrothermal to obtain bright crystalline $PbI_2$ crystals with a facet angle. In the Teflon-lined hydrothermal autoclave, an un-crystallized $PbI_2$ aqueous solution was observed, but we obtained $PbI_2$ crystals for further work.

Table 1 compares the retail prices of $PbI_2$ and chemicals for $PbI_2$ synthesis, depending on the purity. Prices of $PbI_2$ with 98.5%, 99.99%, and 99.9985% purities are 1.47 \$/g, 6.42 \$/g, and 4.33 \$/g, respectively. This comparison shows that a high purity of $PbI_2$ beyond 99% requires a high expenditure. The price of 99.9985% purity of $PbI_2$ is three times higher than that of low-grade $PbI_2$ with 98.5% purity. In contrast, using the mentioned chemicals for $PbI_2$ synthesis, the retail prices are below 10% of the low-grade $PbI_2$ with 98.5% purity. Considering reaction (1) and assuming that researchers would experiment crudely so that only 50% yield would be obtained, the price to obtain crystalized $PbI_2$ could be 0.358 \$/g. Comparing the synthesized $PbI_2$ retail price to low-grade $PbI_2$, it is 24% of the price for low-grade $PbI_2$. Moreover, comparing the synthesized $PbI_2$ retail price to high-grade $PbI_2$, it is only 8.26% of the high-grade $PbI_2$. Even though considering initial costs for the synthesis's tools and systems, the synthesis and purification of $PbI_2$ can be economically feasible for the long-term view and large-scale production. If photophysical properties (for PQDs) or photoconversion efficiencies (for PSCs) would be similar, the prepared $PbI_2$ can be an economical alternative instead of commercially available high-cost $PbI_2$ with high purity.

**Table 1.** Comparison of the retail prices of $PbI_2$ and chemicals for $PbI_2$ synthesis, providing purity [1].

| Purity, Chemical (Brand) | Retail Price, US$ (Quantity (g)) | US$ $g^{-1}$ |
|---|---|---|
| 99.5% $Pb(CH_3COO)_2$, (Fisher Chemical) | 34.38 (250) | 0.138 |
| 99.5%, KI (Samchun Chemicals) | 56.40 (500) | 0.113 |
| 99.99%, trace metals basis, $PbI_2$, (TCI) | 160.43 (25) | 6.42 |
| 99.9985%, metals basis $PbI_2$, (Alfa Aesar) | 108.33 (25) | 4.33 |
| 98.5% $PbI_2$, (Alfa Aesar) | 73.41 (50) | 1.47 |

[1] Chemical price were obtained from chemical companies each.

Firstly, to confirm the synthesized and purified $PbI_2$ as an alternative solution to the high-cost $PbI_2$ with high purity, X-ray diffraction (XRD) patterns and thermogravimetric analysis (TGA) were obtained and performed, respectively, see Figure 1. Figure 1A shows that the crystallized $PbI_2$ exhibits identical patterns, the same as commercially available $PbI_2$, without additional peaks, which can be either a byproduct or the result of degraded products. Compared to reference (PDF# 01-080-1000), hexagonal $PbI_2$ with P-3m1 space group was obtained for all $PbI_2$ chemicals. Even as-synthesized $PbI_2$ without recrystallization and consecutive hydrothermal, XRD patterns match the pattern from commercial $PbI_2$. This result indicates that the crystallized $PbI_2$ structure was obtained, and identical crystallinity was observed when compared to the commercial $PbI_2$.

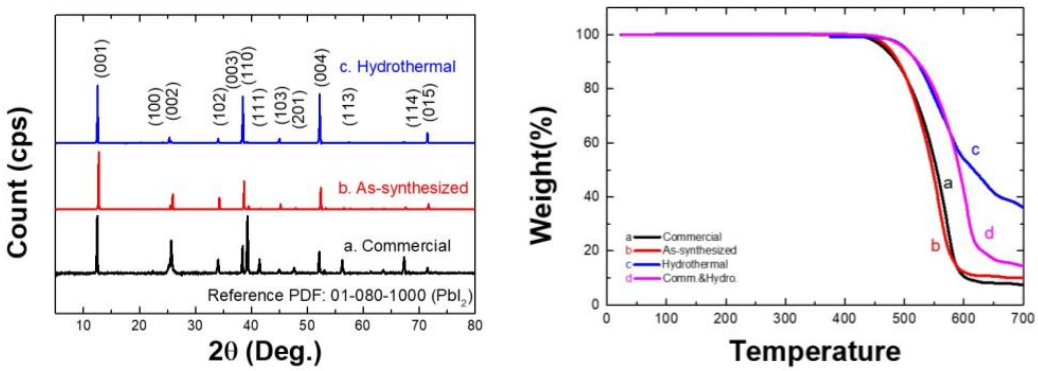


**Figure 1.** (**A**) X-ray diffraction patterns of a. commercially available $PbI_2$ (99.99% purity), b. as-synthesized $PbI_2$ without purification process, and c. crystallized $PbI_2$ after hydrothermal. (**B**) Thermogravimetric analysis (TGA) curves for commercially available $PbI_2$ (99.99% purity), b. as-synthesized $PbI_2$ without purification process, c. crystallized $PbI_2$ after hydrothermal, and d. commercially available $PbI_2$ (99.99% purity) with an additional hydrothermal process for comparison.

Figure 1B presents TGA curves for various $PbI_2$ sources. All $PbI_2$ sources do not decrease their weight up to 400 °C, which implies that there is no hydrated form and residual $H_2O$ in the powder/crystals. Commercially available $PbI_2$ and as-synthesized $PbI_2$ start to lose their weight around 440 °C and the weight loss is generally expected decomposition of $PbI_2$, to metallic $Pb^0$, as follows [33,34]:

$$PbI_{2\,(s)} \rightarrow Pb_{\,(s)} + I_{2\,(g)} \quad (2)$$

The broad weight loss profile implies breaking the bond between Pb-I-Pb coordination and sublimation of $I_2$ occurs. Interestingly, all hydrothermal $PbI_2$ from both commercial and as-synthesized ones start to lose their weight around 500 °C, indicating higher thermal stability of $PbI_2$. We speculate that improving crystallinity provides better thermal stability raising decomposition starting temperature up to 60 °C higher than that of $PbI_2$ without hydrothermal. We expect that the enhanced crystallinity could reduce defects. The enhanced crystallinity could provide better stoichiometric coordination between Pb and I, reducing imbalanced charging sites induced by the missing crystal components, which may decrease regional lattice distortion/strain. Thus, incorporating more thermal energy at a higher temperature would need to distort the Pb-I-Pb coordination to induce the thermal decomposition of $PbI_2$ [33].

Table 2 shows the X-ray fluorescence spectroscopic analysis (XRF) and elemental analysis about Pb and I. Other elements were not able to be measured. Interestingly, the hydrothermal process enhances the I/Pb molar ratio to the two $PbI_2$ from both as-synthesized and commercial sources. During the hydrothermal process, the dissolution of $PbI_2$ in the aqueous solution occurred and crystallization occurred while cooling the Teflon-lined Hydrothermal autoclave [30]. After the crystallization, improvement of iodide components in the $PbI_2$ implies better crystallinity reduces defects, especially iodide-mediated defects. Furthermore, incorporating a higher amount of iodide in the $PbI_2$ can potentially use the larger amount of iodide to fill the iodide medicated vacancies in the perovskite/PQDs, which acts as non-radiative recombination sites.

**Table 2.** X-ray fluorescence spectroscopic analysis of various $PbI_2$ sources.

| $PbI_2$ Sources | Pb (wt%) | I (wt%) | Molar Ratio (I/Pb) |
|---|---|---|---|
| Commercially available | 43.0 | 57.0 | 2.164 |
| As-synthesized (without purification) | 43.2 | 56.8 | 2.147 |
| Hydrothermal (from as-synthesized) | 42.7 | 57.3 | 2.191 |
| Hydrothermal (from commercial) | 42.8 | 57.2 | 2.182 |

### *3.2. Similarity of $CsPbI_3$ Perovskite Quantum Dots' Photophysical Properties and Stabilities Using Either Crystallized $PbI_2$ or Commercial $PbI_2$ with 99.99% Purity*

Figure 2 demonstrates TEM images and SAED patterns of the $CsPbI_3$ PQDs using commercially available $PbI_2$ with 99.99% purity (Figure 2A,C) and crystallized $PbI_2$ (Figure 2B,D). Both PQDs show cubic shapes with similar size and size distributions (11.3 ± 2.0 nm PQDs made from the commercial $PbI_2$, and 11.04 ± 1.23 nm, another PQDs from hydrothermal $PbI_2$, see Figure S1 in supporting information). Note that PQDs made from as-synthesized $PbI_2$ show a similar cubic shape of PQDs but with a slightly smaller size (9.9 ± 1.4 nm, see Figure S2). Also, observing SAED patterns, the two kinds of PQDs show similar patterns to concentric circles and obtained diffractions from multiple PQDs, which imply the presence of (100), (110), (200) planes in the PQDs. The two insets in Figure 2A,C present identical d-spacing for (100). All of the patterns and d-spacing were matched with XRD patterns obtained from the two kinds of PQDs (Figure S3). In the XRD patterns from the two PQDs, major peak positions, full width at half maximums (FWHMs), and peak intensity ratios were identical. The two kinds of PQDs made from the crystallized/commercial $PbI_2$ cannot be distinguished through material characterizations. Therefore, using both commercial/hydrothermal $PbI_2$ produce the identical material quality of PQDs.

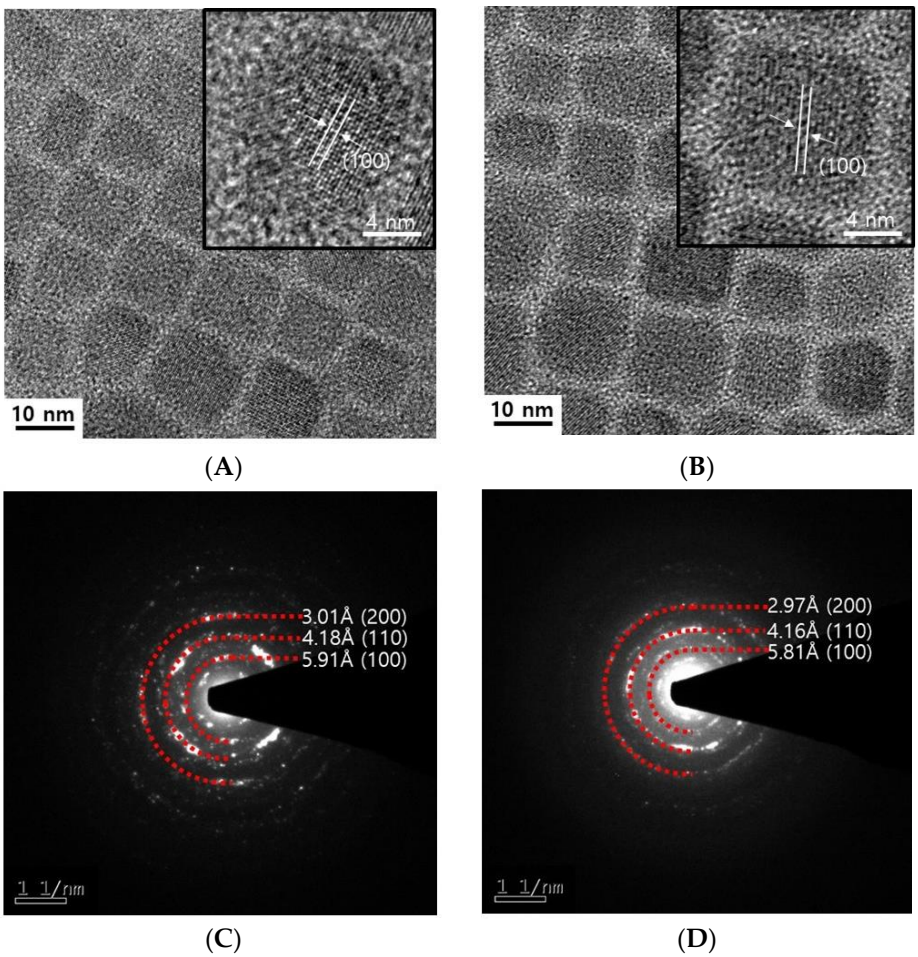


**Figure 2.** (**A**,**B**) Tunneling electron microscopic (TEM) images of (**A**) $CsPbI_3$ perovskite quantum dots (PQDs) with using commercial $PbI_2$ with 99.99% purity and (**B**) with using crystallized $PbI_2$ through hydrothermal. Insets show an enlarged single PQD with lattice fringe. (**C**,**D**) Selected area electron diffraction (SAED) of $CsPbI_3$ PQDs with using commercial $PbI_2$ with 99.99% purity (**C**) and with using crystallized $PbI_2$ through hydrothermal (**D**).

To compare photophysical properties between the two different PQDs, we performed PLQY measurement of the two PQDs with other PQDs made from as-synthesized $PbI_2$. Using as-synthesized, commercial, hydrothermal $PbI_2$ to the PQD synthetic process, PLQY were obtained as 43.00%, 45.83%, 52.61%, respectively. Enhancement of PLQY can be correlated to using iodide enriched $PbI_2$ through the hydrothermal process (Table 2). PLQY is described as follows:

$$PLQY = \frac{k_r}{k_r + k_{nr}}. \quad (3)$$

PLQY of these PQDs consists of two components: radiative decay rate constant ($k_r$) and non-radiative decay rate constant ($k_{nr}$). The $k_r$ is the rate constant for radiative recombination such as photoluminescence in these PQDs, and $k_{nr}$ is for non-radiative recombination such as vibration relaxation related processes. The $k_{nr}$ is calculated by considering various aspects in the PQDs, such as various defects (interstitials, charged/neutral vacancies, antisites, surface, etc.) [35] charge transfer medium. In this work, the increment of iodide components can fill the iodide-vacancy mediated defect. This defect-mediate non-radiative recombination process can be hindered so that overall PLQY can be increased. The control of non-radiative radiative recombination is key to reducing the translation of electron energy to vibration energy of lattice atoms, i.e., phonons, which are sources to induce heat generation. Usage of the more efficient radiation process is also an important factor in enhancing contrast in the display devices. Therefore, increasing PLQY with this additional purification process for precursor is essential to solve the major technical issues, such as reducing internal-generated heat and increasing energy efficiency in the display devices.

We also tested the stability of the two kinds of PQDs; compared to the other PQDs made from as-synthesized $PbI_2$, the initial emission shapes and intensities were maintained (see Figure 3). In contrast, photoluminescence intensities from the other PQDs (made through as-synthesized $PbI_2$) diminished as time goes by, see Figure S4. These PLQY and stability tests, performed through photoluminescence measurements, photophysical properties between the two kinds of PQDs resembled each other; we found that even using hydrothermal $PbI_2$ can reduce production cost by 1/20 (6.42 \$/g for commercial $PbI_2$ vs. 0.358 \$/g for hydrothermal $PbI_2$, see Table 1).

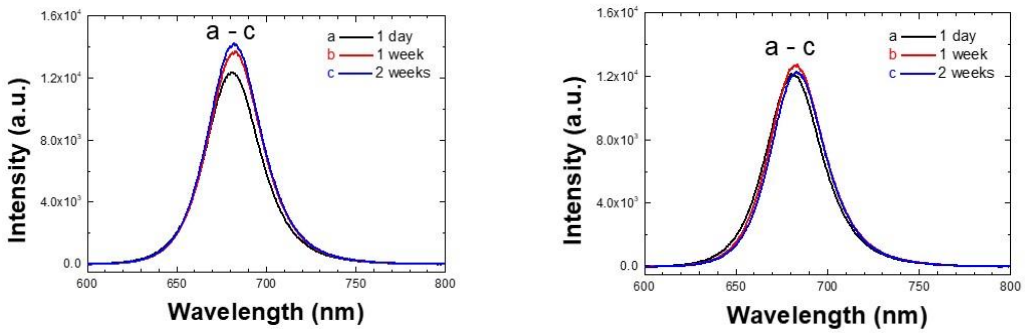


**Figure 3.** (**A**) Photoluminescence spectra obtained emission from the two kinds of $CsPbI_3$ PQDs by using commercial $PbI_2$ with 99.99% purity (**A**) or with using crystallized $PbI_2$ through hydrothermal (**B**). Three emission spectra were obtained on the day when PQDs colloidal dispersed solutions were made (a, black line), one week (b, red line), and two weeks (c, blue line) after the synthesis. The solutions were preserved under $N_2$ gas at 2 °C.

### *3.3. Application of the Hydrothermal Process to Problematic $PbI_2$ to Make Better Quality of $MAPbI_3$ Perovskite Film for Enhanced Photoconversion Efficiency of PSCs*

To clarify the hydrothermal process's effect to cure the unknown dissolving issue, we used problematic $PbI_2$ with 99.999% purity to prepare two $MAPbI_3$ perovskite films, but for one of them, the extra hydrothermal process was applied before using the $PbI_2$ to make

the perovskite film. As shown in Figure 4, bigger grain sizes were obtained by applying the extra hydrothermal process, even using the identical $PbI_2$ with the same purity. In Figure S5, grain sizes got bigger from 179 ± 80 to 255 ± 130 nm (for the longest sizes within a grain) and from 64 ± 25 to 111 ± 60 nm (for shortest sizes within a grain). The grain sizes were enlarged around 42–73% with the addition of an extra hydrothermal process. Figure S6a shows that in this $PbI_2$ with a certain synthetic batch, the $PbI_2$ did not completely dissolve in the mixed solvent of DMF : DMSO (4:1, volume ratio); we cannot determine the reason. With the addition of the hydrothermal process, we improved the solubility of $PbI_2$ in the mixed solvent. Note that most $PbI_2$ dissolve well with MAI by forming lead iodide plumbate complex in the mixed solvent under room temperature, but by applying the hydrothermal process to PbI2, we tried to solve the dissolving issue. Currently, we are doing further investigation to clarify the details of the problematic issue. The presence of the undissolved particles can induce faster crystal film growth at the particle's surface that reacts like a seed, so the particles can cause to skip the necessary process: overcoming an energy barrier to induce the nucleation process. Therefore, relatively smaller grain sizes (~100 nm) were observed in SEM images. In our previous work [36], we obtained larger grains with sizes, about 560 nm). Therefore, the hydrothermal process can obtain a crystallized $PbI_2$ hexagonal structure and reduce lead halide derivates' unwanted species. This work's concentration makes 350 nm $MAPbI_3$ layer thickness (see Figure S7), which is the optimized thickness for efficient $V_{oc}$ and fill factor (FF) from our earlier work [36]. Also, note that the UV-Vis. absorption spectra of $MAPbI_3$ films (see Figure S8) made using commercial $PbI_2$ or crystallized $PbI_2$ show an almost similar absorption trend in the visible region, which indicates an almost identical thickness.

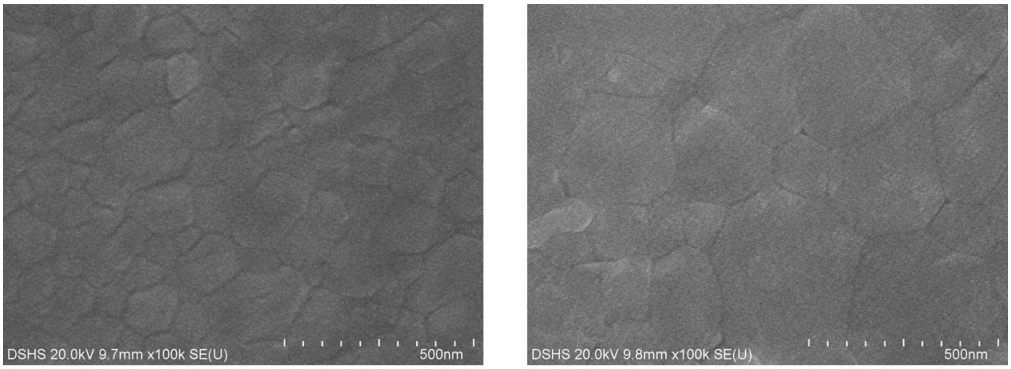


(**A**) (**B**)

**Figure 4.** Scanning electron microscopic (SEM) images of $MAPbI_3$ perovskite films made by using (**A**) different commercial $PbI_2$ (from Alfa Aesar, product # 12,724 Lot # U14E066) and (**B**) the same commercial $PbI_2$ from Alfa Aesar but with the additional hydrothermal process.

In Figure 5 and Table 3, photovoltaic performances of $MAPbI_3$ PSCs are shown with J-V curves. In addition to the hydrothermal process, overall photovoltaic performances increase. By comparing the two best cells in the two cases, we see that hydrothermal addition enhances FF from 72.31 to 75.88. This increment mainly contributes to improving the photoconversion efficiency of PSCs by incorporating the hydrothermal process. From Figure 4, we speculate that enlarged grain size contributes to reducing the series resistance ($R_s$) and increasing shunt resistance ($R_{sh}$) in the PSCs. Even though the average photoconversion efficiencies between the two cases are in the standard deviation, seeing the distribution of the performances carefully in Figure 5A, we observed the positive contribution of the hydrothermal process to enhance the performance of PSCs. We are also conducting research further to improve the overall purification to obtain enhanced performances significantly. However, so far, it is possible to expect similar performances about PQDs and PSCs, by using the synthesized and crystallized $PbI_2$ from low-quality sources instead of commercially available high-purity $PbI_2$.

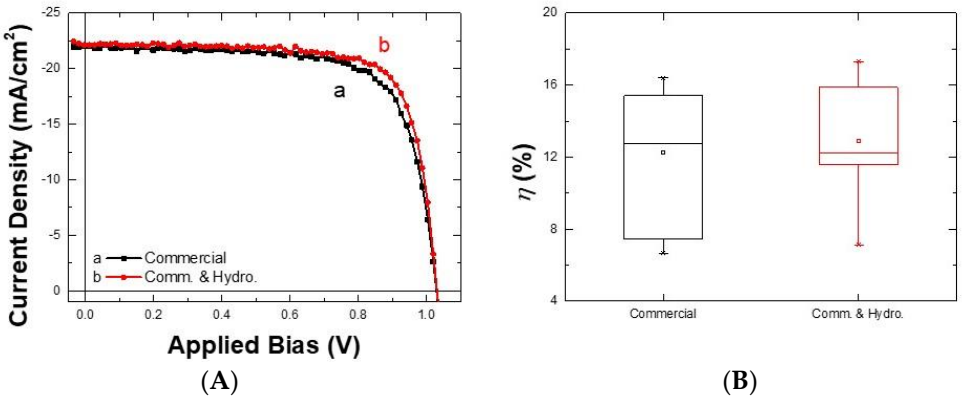


**Figure 5.** (**A**) J-V curves for PSCs with using the commercial $PbI_2$ (a, black trace) and commercial $PbI_2$ with an additional hydrothermal process (b, red trace). (**B**) average and deviation of the photoconversion efficiency of PSCs with the two different $PbI_2$.

**Table 3.** Photovoltaic performances of $MAPbI_3$ perovskite solar cells (PSCs).

| $PbI_2$ Sources | $V_{oc}$ (V) | $J_{sc}$ (mA/cm$^2$) | FF | PCE (%) Best (Average ± stan. dev.) |
|---|---|---|---|---|
| Commercial | 1.029 | 22.03 | 72.31 | 16.39 (14.77 ± 1.82) |
| Commercial with hydrothermal | 1.031 | 22.14 | 75.88 | 17.31 (15.18 ± 1.92) |

## 4. Conclusions

In conclusion, we aimed to develop a strategy to utilize the economically feasible low-grade precursors to obtain a comparable quality of material for the cutting-edge research field, perovskite solar cells, and study the photophysical properties of perovskite quantum dots. Through recrystallization and hydrothermal, from low-grade resources, we obtained similar $PbI_2$ with 99.99% purity, and conducted analyses using XRD, TGA, and XRF. We observed that similar structural but heat-resistible $PbI_2$ was obtained through the purification processes, and the iodide component increases after the purification, which can act by increasing photoluminescence quantum yield filling the iodide defect mediated non-radiative recombination sites. Furthermore, the hydrothermal process can promote solubility of $PbI_2$ into the DMF/DMSO mixed solvent with MAI, so hindering undissolved particle formation helps to grow grain bigger and improve photoconversion efficiencies of perovskite solar cells. This work can provide the strategy to enhance the quality of $PbI_2$ precursor for the fabrication of high-quality perovskite/perovskite quantum dots. Also, this work can contribute to the commercialization of perovskite-based applications.

**Supplementary Materials:** The following are available online at https://www.mdpi.com/1996-1073/14/1/201/s1, Figure S1: Histograms about sizes of PQDs, Figure S2: TEM images of PQDs made through as-synthesized $PbI_2$ without further recrystallization/hydrothermal and their histogram, Figure S3: XRD patterns of PQDs, Figure S4: Photoluminescence spectra of PQDs made through as-synthesized $PbI_2$, Figure S5: Historgrams about grain sizes of perovskite films, Figure S6: Precursor solution (DMF/DMSO mixed) with MAI and $PbI_2$, Figure S7: A typical cross-sectional SEM image of perovskite layer for the PSCs whose performances were shown in Figure 5., Figure S8: UV-Vis. absorption spectra of $MAPbI_3$ films using commercially available $PbI_2$ (99.99 % purity) and crystallized $PbI_2$ after hydrothermal.

**Author Contributions:** S.J.Y., J.K., and J.P. designed the experiments. C.L., Y.S., G.G.J., J.J., D.K., and B.J. performed the experiments. All authors contributed to analyzing the results, data analysis, and preparation of the final manuscript. All authors have read and agreed to the published version of the manuscript.

**Funding:** This work was supported by the 2020 Daegu Science High School Self-motivated Research Projects and National Research Foundation of Korea (NRF) grant funded by the Korean government (MSIT) 2019R1F1A1062395.

**Institutional Review Board Statement:** Not applicable.

**Informed Consent Statement:** Not applicable.

**Data Availability Statement:** Data is contained within the article.

**Acknowledgments:** This work was supported by the 2020 Daegu Science High School Self-motivated Research Projects and National Research Foundation of Korea (NRF) grant funded by the Korean government (MSIT) 2019R1F1A1062395. We thank Hyun Woo Nho for valuable discussions about material characterizations.

**Conflicts of Interest:** The authors declare no conflict of interest.

## References

1. Chang, J.J.; Zhu, H.; Li, B.C.; Isikgor, F.H.; Hao, Y.; Xu, Q.H.; Ouyang, J.Y. Boosting the performance of planar heterojunction perovskite solar cell by controlling the precursor purity of perovskite materials. *J. Mater. Chem. A* **2016**, *4*, 887–893. [CrossRef]
2. Wang, Q.; Zhang, X.S.; Jin, Z.W.; Zhang, J.R.; Gao, Z.F.; Li, Y.F.; Liu, S.Z.F. Energy-Down-Shift CsPbCl3:Mn Quantum Dots for Boosting the Efficiency and Stability of Perovskite Solar Cells. *ACS Energy Lett.* **2017**, *2*, 1479–1486. [CrossRef]
3. Huang, W.X.; Yoon, S.J.; Sapkota, P. Effect of Light Illumination on Mixed Halide Lead Perovskites: Reversible or Irreversible Transformation. *ACS Appl. Energy Mater.* **2018**, *1*, 2859–2865. [CrossRef]
4. Kim, G.; Min, H.; Lee, K.S.; Lee, D.Y.; Yoon, S.M.; Seok, S.I. Impact of strain relaxation on performance of α-formamidinium lead iodide perovskite solar cells. *Science* **2020**, *370*, 108–112. [CrossRef]
5. Asif, A.A.; Singh, R.; Alapatt, G.F. Technical and economic assessment of perovskite solar cells for large scale manufacturing. *J. Renew. Sustain. Energy* **2015**, *7*, 043120. [CrossRef]
6. Mitzi, D.B.; Feild, C.; Schlesinger, Z.; Laibowitz, R. Transport, optical, and magnetic properties of the conducting halide perovskite CH3NH3SnI3. *J. Solid State Chem.* **1995**, *114*, 159–163. [CrossRef]
7. Kagan, C.; Mitzi, D.; Dimitrakopoulos, C. Organic-inorganic hybrid materials as semiconducting channels in thin-film field-effect transistors. *Science* **1999**, *286*, 945–947. [CrossRef]
8. Mitzi, D.B.; Chondroudis, K.; Kagan, C.R. Design, structure, and optical properties of organic− inorganic perovskites containing an oligothiophene chromophore. *Inorg. Chem.* **1999**, *38*, 6246–6256. [CrossRef]
9. Kojima, A.; Teshima, K.; Shirai, Y.; Miyasaka, T. Organometal Halide Perovskites as Visible-Light Sensitizers for Photovoltaic Cells. *J. Am. Chem. Soc.* **2009**, *131*, 6050–6051. [CrossRef]
10. Senanayak, S.P.; Yang, B.; Thomas, T.H.; Giesbrecht, N.; Huang, W.; Gann, E.; Nair, B.; Goedel, K.; Guha, S.; Moya, X. Understanding charge transport in lead iodide perovskite thin-film field-effect transistors. *Sci. Adv.* **2017**, *3*, e1601935. [CrossRef]
11. Dong, Q.; Fang, Y.; Shao, Y.; Mulligan, P.; Qiu, J.; Cao, L.; Huang, J. Electron-hole diffusion lengths >175 μm in solution-grown CH3NH3PbI3 single crystals. *Science* **2015**, *347*, 967–970. [CrossRef] [PubMed]
12. Wang, B.; Iocozzia, J.; Zhang, M.; Ye, M.; Yan, S.; Jin, H.; Wang, S.; Zou, Z.; Lin, Z. The charge carrier dynamics, efficiency and stability of two-dimensional material-based perovskite solar cells. *Chem. Soc. Rev.* **2019**, *48*, 4854–4891. [CrossRef] [PubMed]
13. Saba, M.; Cadelano, M.; Marongiu, D.; Chen, F.; Sarritzu, V.; Sestu, N.; Figus, C.; Aresti, M.; Piras, R.; Lehmann, A.G. Correlated electron–hole plasma in organometal perovskites. *Nat. Commun.* **2014**, *5*, 1–10. [CrossRef] [PubMed]
14. Jeon, N.J.; Noh, J.H.; Kim, Y.C.; Yang, W.S.; Ryu, S.; Seok, S.I. Solvent engineering for high-performance inorganic-organic hybrid perovskite solar cells. *Nat. Mater.* **2014**, *13*, 897–903. [CrossRef]
15. Zhang, Y.; Kim, S.G.; Lee, D.K.; Park, N.G. $CH_3NH_3PbI_3$ and $HC(NH_2)(2)PbI_3$ Powders Synthesized from Low-Grade $PbI_2$: Single Precursor for High-Efficiency Perovskite Solar Cells. *ChemSusChem* **2018**, *11*, 1813–1823. [CrossRef]
16. Saidaminov, M.I.; Abdelhady, A.L.; Murali, B.; Alarousu, E.; Burlakov, V.M.; Peng, W.; Dursun, I.; Wang, L.F.; He, Y.; Maculan, G.; et al. High-quality bulk hybrid perovskite single crystals within minutes by inverse temperature crystallization. *Nat. Commun.* **2015**, *6*, 7586. [CrossRef]
17. Gu, Z.K.; Huang, Z.D.; Li, C.; Li, M.Z.; Song, Y.L. A general printing approach for scalable growth of perovskite single-crystal films. *Sci. Adv.* **2018**, *4*, eaat2390. [CrossRef]
18. Bush, K.A.; Frohna, K.; Prasanna, R.; Beal, R.E.; Leijtens, T.; Swifter, S.A.; McGehee, M.D. Compositional Engineering for Efficient Wide Band Gap Perovskites with Improved Stability to Photoinduced Phase Segregation. *ACS Energy Lett.* **2018**, *3*, 428–435. [CrossRef]
19. Noh, J.H.; Im, S.H.; Heo, J.H.; Mandal, T.N.; Seok, S.I. Chemical Management for Colorful, Efficient, and Stable Inorganic-Organic Hybrid Nanostructured Solar Cells. *Nano Lett.* **2013**, *13*, 1764–1769. [CrossRef]
20. Wakamiya, A.; Endo, M.; Sasamori, T.; Tokitoh, N.; Ogomi, Y.; Hayase, S.; Murata, Y. Reproducible Fabrication of Efficient Perovskite-based Solar Cells: X-ray Crystallographic Studies on the Formation of CH3NH3PbI3 Layers. *Chem. Lett.* **2014**, *43*, 711–713. [CrossRef]

21. Sadhanala, A.; Ahmad, S.; Zhao, B.; Giesbrecht, N.; Pearce, P.M.; Deschler, F.; Hoye, R.L.; Gödel, K.C.; Bein, T.; Docampo, P. Blue-green color tunable solution processable organolead chloride–bromide mixed halide perovskites for optoelectronic applications. *Nano Lett.* **2015**, *15*, 6095–6101. [CrossRef] [PubMed]
22. Jia, Y.; Kerner, R.A.; Grede, A.J.; Brigeman, A.N.; Rand, B.P.; Giebink, N.C. Diode-pumped organo-lead halide perovskite lasing in a metal-clad distributed feedback resonator. *Nano Lett.* **2016**, *16*, 4624–4629. [CrossRef] [PubMed]
23. Huang, H.; Pradhan, B.; Hofkens, J.; Roeffaers, M.B.; Steele, J.A. Solar-Driven Metal Halide Perovskite Photocatalysis: Design, Stability, and Performance. *ACS Energy Lett.* **2020**, *5*, 1107–1123. [CrossRef]
24. Kim, I.S.; Pellin, M.J.; Martinson, A.B. Acid-compatible halide perovskite photocathodes utilizing atomic layer deposited $TiO_2$ for solar-driven hydrogen evolution. *ACS Energy Lett.* **2019**, *4*, 293–298. [CrossRef]
25. Suarez, I.; Valles-Pelarda, M.; Gualdron-Reyes, A.F.; Mora-Sero, I.; Ferrando, A.; Michinel, H.; Salgueiro, J.R.; Pastor, J.P.M. Outstanding nonlinear optical properties of methylammonium- and Cs-PbX3 (X = Br, I, and Br-I) perovskites: Polycrystalline thin films and nanoparticles. *APL Mater.* **2019**, *7*, 041106. [CrossRef]
26. Yangi, L.K.; Li, Y.W.; Pei, Y.X.; Wang, J.Q.; Lin, H.; Li, X. A novel 2D perovskite as surface "patches " for efficient flexible perovskite solar cells. *J. Mater. Chem. A* **2020**, *8*, 7808–7818. [CrossRef]
27. Zhou, N.J.; Bekenstein, Y.; Eisler, C.N.; Zhang, D.D.; Schwartzberg, A.M.; Yang, P.D.; Alivisatos, A.P.; Lewis, J.A. Perovskite nanowire-block copolymer composites with digitally programmable polarization anisotropy. *Sci. Adv.* **2019**, *5*, eaav8141. [CrossRef]
28. Chen, L.-C.T.; Tien, C.-H.; Tseng, Z.-L.; Ruan, J.-H. Enhanced Efficiency of $MAPbI_3$ Perovskite Solar Cells with $FAPbX_3$ Perovskite Quantum Dots. *Nanomaterials* **2019**, *9*, 121. [CrossRef]
29. Liu, F.; Zhang, Y.H.; Ding, C.; Kobayashi, S.; Izuishi, T.; Nakazawa, N.; Toyoda, T.; Ohta, T.; Hayase, S.; Minemoto, T.; et al. Highly Luminescent Phase-Stable CsPbI(3) Perovskite Quantum Dots Achieving Near 100% Absolute Photoluminescence Quantum Yield. *ACS Nano* **2017**, *11*, 10373–10383. [CrossRef]
30. Zhu, X.H.; Wangyang, P.H.; Sun, H.; Yang, D.Y.; Gao, X.Y.; Tian, H.B. Facile growth and characterization of freestanding single crystal $PbI_2$ film. *Mater. Lett.* **2016**, *180*, 59–62. [CrossRef]
31. Koziol, J. Studies on Flavins in Organic Solvents-i*. Spectral Characteristics of Riboflavin, Riboflavin Tetrabutyrate and Lumichrome. *Photochem. Photobiol.* **1966**, *5*, 41–54. [CrossRef]
32. Golden Rain. Available online: https://edu.rsc.org/exhibition-chemistry/golden-rain/2000048.article (accessed on 20 December 2020).
33. Malevu, T.D.; Ocaya, R.O.; Tshabalala, K.G. Phase transformations of high-purity $PbI_2$ nanoparticles synthesized from lead-acid accumulator anodes. *Phys. B Condens. Matter* **2016**, *496*, 69–73. [CrossRef]
34. Dualeh, A.; Gao, P.; Seok, S.I.; Nazeeruddin, M.K.; Graetzel, M. Thermal Behavior of Methylammonium Lead-Trihalide Perovskite Photovoltaic Light Harvesters. *Chem. Mater.* **2014**, *26*, 6160–6164. [CrossRef]
35. Ten Brinck, S.; Zaccaria, F.; Infante, I. Defects in Lead Halide Perovskite Nanocrystals: Analogies and (Many) Differences with the Bulk. *ACS Energy Lett.* **2019**, *4*, 2739–2747. [CrossRef]
36. Kim, J.; Park, B.W.; Baek, J.; Yun, J.S.; Kwon, H.W.; Seidel, J.; Min, H.; Coelho, S.; Lim, S.; Huang, S.J. Unveiling the Relationship between the Perovskite Precursor Solution and the Resulting Device Performance. *J. Am. Chem. Soc.* **2020**, *142*, 6251–6260. [CrossRef]